Vision-Based Leader–Follower Formation Control of Multiagents With Visibility Constraints

Xiaomei Liu, Shuzhi Sam Ge, *Fellow, IEEE*, and Cher-Hiang Goh, *Senior Member, IEEE*

***Abstract*— In this brief, a vision-based tracking scheme is studied for the leader–follower formation control of multiagent system under visibility constraints without communication among agents. A kinect is the sole sensor installed on each agent to estimate the pose, including relative orientations and relative positions of the local leader. A dipolar vector field is established to generate and maintain a desired formation given the desired displacement on positions among agents. The visibility constraints of kinect are converted into input constrains given the pose of the local leader, and an auxiliary system is designed to analyze the effect of visibility constraints. Combining the state of the auxiliary system with the vector filed, the proposed control protocol is able to achieve the formation tracking without global or local communication among agents. Simulation studies on the robot operating system using the Gazebo simulator and experimental results on Turtlebot2 are presented to illustrate the performance of the proposed approaches.**

***Index Terms*— Dipolar vector field, leader–follower (L-F) formation control, multiagent system (MAS), visibility maintenance, vision-based pose estimation.**

I. Introduction

VISION-BASED control has attracted increasing attention in recent years, and it is not restricted to formation control, such as collision avoidance [1] and target tracking [2]. Cameras have been strongly tied to robotic applications benefiting from their low prices and sufficient information they can capture compared with conventional sensors, e.g., laser range finders and sonars. A framework for the vision-based formation control was proposed in [3]. Panagou and Kumar [4] studied the formation control of multiple robots with visibility and communication constraints based on vision. In [5], the leader–follower (L-F) formation control of mobile robots without communication was solved by using a pan-controlled camera as the sole sensor. In [6], a vision-based localization protocol for the L-F formation control of unicycle robots equipped with a panoramic camera was proposed, whereas the necessary conditions of observability was discussed. Similar schemes for the vision-based formation control were also proposed in [7]–[9]. On the other hand, some work explores the potential of applying global vision sensor for solutions. In [10], the position and the orientation of robots were estimated by a global vision system that can cover whole area for the formation control. A similar achievement was also reported in [11]. Reference [12] studied the effects of different visual feedbacks with multiple cameras on the performance of human operators to achieve swarm of multiple unmanned aerial vehicles.

The essential problem for the formation control using onboard cameras is to estimate the pose of the robot with respect to a reference frame. Despite the progresses achieved, this topic remains challenging, because traditional cameras provide the view-angles to an object but not distances. Kinect, featureing both RGB camera and depth sensor, provides a solution to this problem. A few publications have reported the applications of kinect on the cooperative control of multiagent system (MAS) [13] but far from being desired. First, the commonly estimated information via kinect is distance at most the angle of an object relative to the center of the kinect, which renders that the criteria of the formation has to be weaken (e.g., to control the follower to keep desired distance from the leader). Most of existing solutions needed the combination of multiple sensors for desired performance. From a localization viewpoint, at least three landmarks (better be static) should be equipped, which is not easily achievable in kinect-based formation without information sharing. Due to the limited range of view of kinect or specific formation shape such as pseudo V, there is normally one leader agent detected in field of vision. Meanwhile, it is practically impossible to keep the visibility of multiple visual targets in the whole procedure. Hence, the exploration of the solution for the rigid formation of MAS with the sole on-board cameras is still challenging.

The L-F formation control is commonly considered in the situation where agents are subject to limited sensing and communication and lack of localization in global coordination [14], [15]. The limited field of view challenges the success of the formation control via onboard kinect. Efforts have been made to deal with visibility of fixed landmarks for the navigation problem of mobile robots with limited sensing [16] and visual servoing control [17]. However, few studies have aimed at visibility constraints in formation control, where the objective enhances the difficulty of visibility maintenance, since both the agent itself and the visual target are mobile. To maintain the visibility especially when a specific displacement on the pose with respect to the mobile object (e.g., leader) has to be kept, the relative pose or motion of the mobile target should be accurately estimated visually

Manuscript received May 3, 2017; revised November 12, 2017; accepted January 1, 2018. Date of publication January 25, 2018; date of current version April 11, 2019. Manuscript received in final form January 4, 2018. Recommended by Associate Editor A. Serrani. *(Corresponding author: Shuzhi Sam Ge.)*

X. Liu and S. S. Ge is with the Department of Electrical and Computer Engineering, National University of Singapore, Singapore 117576 (e-mail: samge@nus.edu.sg).

C.-H. Goh is with the Department of Electrical and Computer Engineering, National University of Singapore, Singapore 117576, and also with the DSO National Laboratories, Singapore 118230.

Color versions of one or more of the figures in this paper are available online at http://ieeexplore.ieee.org.

Digital Object Identifier 10.1109/TCST.2018.2790966

as feedback massages. In addition, it remains unexplored that how to incorporate these feedback messages into the controller design as the bearing angular is not commonly involved in the agent's system dynamics.

Motivated by the issue of the vision-based formation control, the L-F formation tracking of MAS using kinect as the sole sensor under visibility constraints without communication among agents is addressed for the first time in this brief. The kinect has dual role in this scheme, one as the sensor to detect the pose of the leader, and another one as the orientational indicator for the follower, which replaces the usage of a gyroscopes or acceleration sensors. The body-fixed frame of the leader agent can be set up with one landmark.

The primary contribution is the proposal of a vision-based pose estimation method with RGBD images captured by the individual kinect board on the follower required for the formation control and visibility maintenance. This is difficult to be achieved by sole traditional sensors (e.g., laser rangefinder and sonar). Consequently, the formation tracking based on predefined position displacement between agents is able to be realized with consensus in motion direction provided the kinect on each agent. The visibility constraints of kinect are converted into a set of input constraints. An auxiliary design system is presented to analyze the effect of visibility constraints, and states of auxiliary design system are utilized to compensate the formation controller ensuring the formation keeping under visibility maintenance.

II. Mathematical Modeling

Before proceeding further, the following definitions are made in this brief.

Definition 1 (Global Leader): In MAS, the agent that has the knowledge of the desired trajectory or is assigned the task of the environment exploration is defined as the *Global Leader*.

Definition 2 (Local Leader): In MAS, the agent which is in the range of visibility of another agent and selected to be the formation reference of this agent is defined as the *local leader* of this agent.

A. System Dynamics

Consider a network of MASs $V = \{v_1, \ldots, v_N\}$, where $v_i (i = 1, \ldots, N)$ represents ith agent in the network and N is the number of agents.

Assumption 1: Without loss of generality, it is assumed that the first agent v_1 is the global leader for the given task, who knows the desired trajectory, whereas other agents know only which agent is the leader and the desired position displacement to achieve predefined formation.

We assume N agents with similar motions with respect to a global frame $\mathcal{G}$ described by the following equation:

$$\dot{\mathbf{q}}_{0i} = \begin{bmatrix} \cos\theta_i & 0 \\ \sin\theta_i & 0 \\ 0 & 1 \end{bmatrix} \mathbf{u}_i \Rightarrow \begin{bmatrix} \dot{x}_{0i} \\ \dot{y}_{0i} \\ \dot{\theta}_i \end{bmatrix} = \begin{bmatrix} \cos\theta_i & 0 \\ \sin\theta_i & 0 \\ 0 & 1 \end{bmatrix} \begin{bmatrix} \nu_i \\ \omega_i \end{bmatrix} \tag{1}$$

where $\mathbf{q}_{0i} = [x_{0i} \quad y_{0i} \quad \theta_i]^T$ is the configuration vector of agent v_i, $\mathbf{r}_{0i} = [x_{0i} \quad y_{0i}]^T$ represents the position of agent v_i in the world coordinate system, and θ_i is the orientation of agent v_i with respect to $\mathcal{G}$; $\mathbf{u}_i = [\nu_i \quad \omega_i]^T$ is the system input (ν_i and ω_i are linear and angular velocity of agent v_i, respectively). To mathematically express the motion of the follower v_i with respect to the leader' body-fixed frame $\mathcal{J}$ ($\mathcal{J} = 1, \ldots, N$), write the position of the follower v_i with respect to its a local leader frame $\mathcal{J}$ as $\mathbf{r}_i = [x_i \quad y_i]^T$, given as $\mathbf{r}_i = R(-\theta_i)(\mathbf{r}_i - \mathbf{r}_j)$. The time derivative of $\mathbf{r}_i$ is

$$\dot{\mathbf{r}}_i = \dot{\mathbf{R}}(-\theta_j)(\mathbf{r}_i - \mathbf{r}_j) + \mathbf{R}(-\theta_j)(\dot{\mathbf{r}}_i - \dot{\mathbf{r}}_j) \tag{2}$$

where

$$\mathbf{R}(-\theta_j) = \begin{bmatrix} \cos\theta_j & \sin\theta_j \\ -\sin\theta_j & \cos\theta_j \end{bmatrix} \tag{3}$$

is the rotation matrix of the body-fixed frame $\mathcal{J}$ with respect to frame $\mathcal{G}$, and

$$\dot{\mathbf{R}}(\theta_j) = \begin{bmatrix} 0 & \omega_j \\ -\omega_j & 0 \end{bmatrix} \mathbf{R}(-\theta_j). \tag{4}$$

Substituting (1) and (3)–(4) into (2), we can get

$$\begin{bmatrix} \dot{x}_i \\ \dot{y}_i \end{bmatrix} = \begin{bmatrix} -1 & y_i \\ 0 & -x_i \end{bmatrix} \begin{bmatrix} \nu_j \\ \omega_j \end{bmatrix} + \begin{bmatrix} \cos(\theta_i - \theta_j) \\ \sin(\theta_i - \theta_j) \end{bmatrix} \nu_i. \tag{5}$$

Define $\beta_i \triangleq \theta_i - \theta_j$, whose time differentiating can be written as

$$\dot{\beta}_i = \dot{\theta}_i - \dot{\theta}_j = \omega_i - \omega_j. \tag{6}$$

Combining (5) and (6) outputs the local system dynamics as

$$\begin{bmatrix} \dot{x}_i \\ \dot{y}_i \\ \dot{\beta}_i \end{bmatrix} = \begin{bmatrix} \cos\beta_i & 0 \\ \sin\beta_i & 0 \\ 0 & 1 \end{bmatrix} \mathbf{u}_i + \begin{bmatrix} -1 & y_i \\ 0 & -x_i \\ 0 & -1 \end{bmatrix} \mathbf{u}_j \tag{7}$$

where $\mathbf{u}_i = [\nu_i \quad \omega_i]^T$ and $\mathbf{u}_j = [\nu_j \quad \omega_j]^T$ are the control inputs of the follower v_i and its local leader v_j.

Assumption 2: There exists a constant $\nu_{\max}$ such that $0 \leq |\nu_i| \leq \nu_{\max} < \infty$ and another constant $\omega_{\max}$ such that $0 \leq |\omega_i| \leq \omega_{\max} < \infty$, $i = 1, \ldots, N$, due to physical constraints. Each agent has *a priori* knowledge on the velocity bounds $\nu_{\max}$ and $\omega_{\max}$.

B. Formation Definition

The formation pattern at time t is defined to be a set of desired displacement $\mathcal{P}(t) = \{\delta_2(t), \ldots, \delta_N(t)\}$ for followers $v_i, i = 2, \ldots, N$ with respect to the local leader frame $\mathcal{J}$, where $\delta_i(t)$ is the desired position displacement of the agent v_i at time t relative to its leader v_j, such that:

$$\left[x_i^{\mathrm{d}} \quad y_i^{\mathrm{d}} \quad \beta_i^{\mathrm{d}}\right]^T = [\delta_{xi} \quad \delta_{yi} \quad 0]^T \tag{8}$$

where $\mathbf{r}_i = [x_i^{\mathrm{d}} \quad y_i^{\mathrm{d}}]^T$ is the desired formation position vector, β_i^{d} is the desired tracking orientation, and $\delta_i = [\delta_{xi} \quad \delta_{yi}]^T$ is the desired displacement of agent v_i at time t with respect to the local leader frame $\mathcal{J}$. We set $\beta_i^{\mathrm{d}} = 0$ indicating that the consensus of MAS in motion direction is required to be achieved such that $\theta_i = \theta_j (i = 2, \ldots, N)$ will be realized with respect to the global frame $\mathcal{G}$.

The formation error for the follower $v_i, i = 2, \ldots, N$ is written as $[\varepsilon_{xi} \quad \varepsilon_{yi}]^T = [x_i - \delta_{xi} \quad y_i - \delta_{yi}]^T$, where $\varepsilon_i = [\varepsilon_{xi} \varepsilon_{yi}]^T$ is the vector of formation errors with respect to the leader frame $\mathcal{J}$.

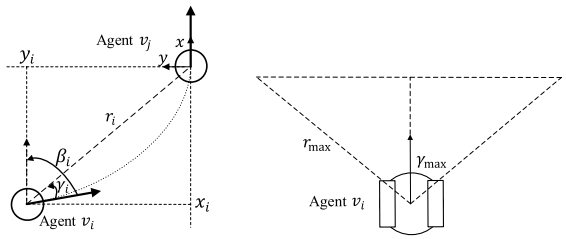

(a) (b)

Fig. 1. Visibility constraints. (a) Vision-based localization. (b) Visual detection range.

C. Visibility Constraints

The information exchanges among agents via forward-looking vision can be modeled by directed graphs. A directed graph G is a pair (V, E), where $V = \{v_1, \ldots, v_N\}$ is a nonempty finite node set and $E \subseteq V \times V$ is an edge set of ordered pairs of nodes, called edges.

Assume that each follower is equipped with a fixed onboard kinect with a limited angle of view $2\gamma_{\max} < \pi$ and all kinects equipped are holonomic. The limited sensing region is modeled as a cone of view, which essentially is an isosceles triangle in obstacle-free environments. The follower v_i is localized with respect to its local leader v_j, i.e., that the displacement in x-coordinate and y-coordinate of $\mathcal{J}$ and the relative orientation β_i or the bearing angle $\gamma_i \in [-\gamma_{\max}, \gamma_{\max}]$ that are measured as shown in Fig. 1(a). Defining the relative distance as $r_i = (x_i^2 + y_i^2)^{1/2}$, an agent has a limited visual detection range such that an object can only be detected if the following conditions can be satisfied that:

$$|\gamma_i| \leq \gamma_{\max} \quad \& \quad \|\mathbf{r}_i\| \leq \frac{r_{\max} \cos \gamma_{\max}}{|\cos \gamma_i|} \tag{9}$$

where $r_{\max}$ is the length of the equal sides of the cone of view. The available detection region of an agent is illustrated in Fig. 1(b).

Assumption 3: A follower can reliably detect its local leader which lies within a limited region with respect to the forward-looking direction.

Assumption 4: The subgraph G_s associated with the followers is directed, and in the graph G, the leader has directed paths to all followers. (Equivalently, G contains a directed spanning tree with the leader as the root.)

Remark 1: There may be more than one agent in the visible range of followers. Selected a specific agent in the field of vision as the local leader in the beginning of a task, this role will not be changed during the task without human intervention. Thus, the specific task for a follower is to track its local leader with specific position displacement while maintaining visibility of the local leader.

III. Formation Control

A. Formation Following

In this brief, a dipolar vector field [18] will be built for each follower to achieve the desired formation with respect to the local leader frame $\mathcal{J}$ as (8). A vector field $\mathbf{F} : \mathbb{R}^2 \to \mathbb{R}^2$ is mathematically built as $\mathbf{F}_i(\varepsilon_i) = 3(\mathbf{p}^T \varepsilon_i)\varepsilon_i - \mathbf{p}(\varepsilon_i^T \varepsilon_i)$, where $\mathbf{p} = [p_x \quad p_y]^T$, $\mathbf{p} \neq 0$. All integral lines in the vector field converge to the original $(0, 0)$ parallel to the axis the $\mathbf{p}$ lies on. To achieve the desired formation of the follower with respect to the local leader frame $\mathcal{J}$ with consensus in motion direction, we choose that $\mathbf{p} = [1 \quad 0]^T$ such that $\varphi_p \triangleq \text{atan2}(p_y, p_x) = 0$ with $p_x = 1$ and $p_y = 0$. The analytical formation of the vector field components F_{xi} and F_{yi} for agent v_i is $F_{xi} = 2\varepsilon_{xi}^2 - \varepsilon_{yi}^2$ and $F_{yi} = 3\varepsilon_{xi}\varepsilon_{yi}$. The corresponding controller $\mathbf{u}_{0i} = [\nu_{0i} \quad \omega_{0i}]^T$ for v_i is proposed as

$$\nu_{0i} = -k_1 \text{sgn}\left(\varepsilon_i^T \begin{bmatrix} \cos\beta_i \\ \sin\beta_i \end{bmatrix}\right) \|\varepsilon_i\| - \text{sgn}\left(\varepsilon_{xi}\right) \nu_{\max} \tag{10}$$

$$\omega_{0i} = -k_2 \left(\beta_i - \varphi_i\right) + \dot{\varphi}_i \tag{11}$$

where ν_{0i} and ω_{0i} denote linear and angular velocity, respectively, $\varphi_i \triangleq \text{atan2}(F_{yi}, F_{xi})$ is the orientation of the vector field at (x_i, y_i), and k_1 and k_2 are two positive scalars.

B. Visibility Maintenance

Given that the local leader is decided among the visible agents in the beginning of the task, the visibility constraints modeled in (9) must be satisfied initially as

$$|\gamma_i(0)| \leq \gamma_{\max} \quad \& \quad \|\mathbf{r}_i(0)\| \leq \frac{r_{\max} \cos \gamma_{\max}}{|\cos \gamma_i(0)|} \tag{12}$$

for $i = 2, \ldots, N$. In the following, the visibility constraints will be divided into two sections, the bearing angle constraint, and the distance constraint and analyzed, respectively. First, the bearing angle constraint can be equally written as $-\gamma_{\max} \leq \gamma_i \leq \gamma_{\max}$. Define $\alpha_i \triangleq \arctan\left(y_i / x_i\right)$, we have

$$\alpha_i = \arctan\left(\frac{\varepsilon_{yi} + \delta_{yi}}{\varepsilon_{xi} + \delta_{xi}}\right) \quad \& \quad \beta_i = \alpha_i - \gamma_i \tag{13}$$

as shown in Fig. 2(c). Converting the constraint on γ_i into the constraint on β_i yields $\beta_i^-(t) \leq \beta_i \leq \beta_i^+(t)$, with

$$\beta_i^-(t) = \alpha_i - \gamma_{\max} \quad \& \quad \beta_i^+(t) = \alpha_i + \gamma_{\max} \tag{14}$$

which are time-varying state constraints. The first part of (12) which implies that the following constraints can be obtained initially that $\beta_i^-(0) \leq \beta_i(0) \leq \beta_i^+(0)$. Based on the first part of (12), the two-sided inequalities of the motion constraints are converted following the procedures in the following. Choose positive scalar k_3 and consider the scalar $\dot{\beta}_i$ regulated as

$$-k_3\left(\beta_i - \beta_i^-\right) + \dot{\beta}_i^- \leq \dot{\beta}_i \leq -k_3\left(\beta_i - \beta_i^+\right) + \dot{\beta}_i^+. \tag{15}$$

Considering that $\dot{\beta}_i = \omega_i - \omega_j$, the above-mentioned inequality can be rewritten as the input constraints as

$$-k_3\left(\beta_i - \beta_i^-\right) + \dot{\beta}_i^- + \omega_j \leq \omega_i \leq -k_3\left(\beta_i - \beta_i^+\right) + \dot{\beta}_i^+ + \omega_j \tag{16}$$

where we have $\dot{\beta}_i^-(t) = \dot{\beta}_i^+(t) = \dot{\alpha}_i$ deducing the input constraints as

$$-k_3\left(\beta_i - \beta_i^-\right) + \dot{\alpha}_i + \omega_j \leq \omega_i \leq -k_3\left(\beta_i - \beta_i^+\right) + \dot{\alpha}_i + \omega_j. \tag{17}$$

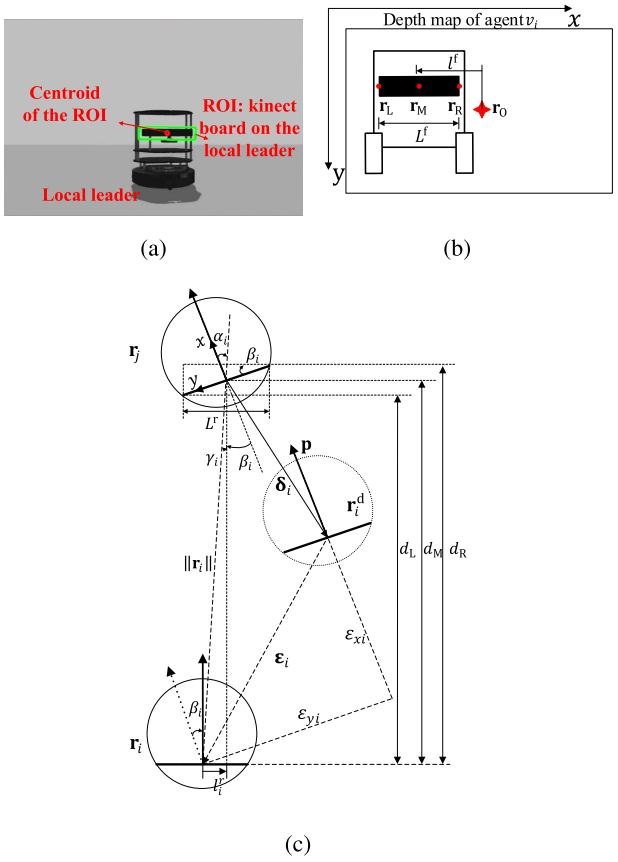

Fig. 2. Vision-based pose estimation. (a) Visual tracking in Gazebo. (b) Vision map. (c) Variables in a local leader frame.

Without the estimation of ω_j, this constraint is further strengthened as

$$-k_3\left(\beta_i-\beta_i^-\right)+\dot{\alpha}_i+\omega_{\max} \le \omega_i \le -k_3\left(\beta_i-\beta_i^+\right)+\dot{\alpha}_i-\omega_{\max}. \quad (18)$$

Meanwhile, it should be satisfied that $\omega_{\max} < \frac{1}{2}k_3(\beta_i^+-\beta_i^-) = k_3\gamma_{\max}$. Considering the presence of input constraints on ω_i and defining

$$\omega_i^- = -k_3\left(\beta_i-\beta_i^-\right)+\dot{\alpha}_i+\omega_{\max} \quad (19)$$

$$\omega_i^+ = -k_3\left(\beta_i-\beta_i^+\right)+\dot{\alpha}_i-\omega_{\max} \quad (20)$$

we have the following input saturation function:

$$S(\omega_i)=\begin{cases}\omega_i^- & \text{if } \omega_i < \omega_i^- \quad (21)\\ \omega_i^+ & \text{if } \omega_i > \omega_i^+ \quad (22)\\ \omega_i & \text{otherwise.} \quad (23)\end{cases}$$

Similar to [19], defining $\Delta\omega_i = S(\omega_i)-\omega_i$, the control scheme on the angular velocity (11) is redesigned as

$$\omega_i = -k_2\left(\beta_i-\varphi_i\right)+\dot{\varphi}_i-\zeta_{1i} \quad (24)$$

with the auxiliary design system chosen as

$$\dot{\zeta}_{1i}=\begin{cases}-k_4\zeta_{1i}-\dfrac{|\left(\beta_i-\varphi_i\right)\Delta\omega_i|+0.5\Delta\omega_i^2}{\|\zeta_{1i}\|^2}\zeta_{1i}+\Delta\omega_i & \\ \qquad\qquad \text{if } |\zeta_{1i}| \ge \chi_1 \quad (25)\\ 0 \qquad\qquad \text{if } |\zeta_{1i}| < \chi_1 \quad (26)\end{cases}$$

where $k_4 > 0$, χ_1 is a small positive value, and $\zeta_{1i} \in \mathbb{R}$ is the state of the auxiliary design system. Then studying the distance constraint, define $R_i^{\max} = r_{\max}\cos\gamma_{\max}/|\cos\gamma_i|$, and we have the distance constraint as $r_i \triangleq \|\mathbf{r}_i\| = (x_i^2+y_i^2)^{1/2} \le R_i^{\max}$. The time derivative of r_i is

$$\dot{r}_i = \left(x_i\dot{x}_i+y_i\dot{y}_i\right)/r_i. \quad (27)$$

Substituting (7) into (27), we obtain

$$\dot{r}_i = \frac{x_i(-v_j+y_i\omega_j+v_i\cos\beta_i)}{r_i}+\frac{y_i(-x_i\omega_j+v_i\cos\beta_i)}{r_i} = -v_i\cos\gamma_i+v_j\cos\alpha_i. \quad (28)$$

Following the similar steps mentioned previously, choose positive scalar k_5 and consider the scalar $\dot{r}_i$ regulated as:

$$\dot{r}_i < -k_5\left(r_i-R_i^{\max}\right)+\dot{R}_i^{\max}. \quad (29)$$

Combining (28) and (29), we obtain

$$v_i > \frac{1}{\cos\gamma_i}\left[k_5\left(r_i-R_i^{\max}\right)-\dot{R}_i^{\max}+v_j\cos\alpha_i\right]. \quad (30)$$

Without the estimation of v_j, this constraint is further strengthened as

$$v_i > \frac{1}{\cos\gamma_i}\left[k_5\left(r_i-R_i^{\max}\right)-\dot{R}_i^{\max}+v_{\max}\cos\alpha_i\right]. \quad (31)$$

Considering the presence of input constraints on v_i and defining

$$v_i^- = \frac{1}{\cos\gamma_i}\left[k_5\left(r_i-R_i^{\max}\right)-\dot{R}_i^{\max}+v_{\max}\cos\alpha_i\right] \quad (32)$$

we have

$$S(v_i)=\begin{cases}v_i^- & \text{if } v_i < v_i^- \quad (33)\\ v_i & \text{otherwise.} \quad (34)\end{cases}$$

Defining $\Delta v_i = S(v_i)-v_i$, the control scheme on the linear velocity (10) is redesigned as

$$v_i = -k_1\text{sgn}\left(\varepsilon_i^T\begin{bmatrix}\cos\beta_i\\ \sin\beta_i\end{bmatrix}\right)\|\varepsilon_i\|-\text{sgn}\left(\varepsilon_{xi}\right)v_{\max}-\zeta_{2i} \quad (35)$$

with the auxiliary design system proposed as

$$\dot{\zeta}_{2i}=\begin{cases}-k_6\zeta_{2i}-\dfrac{\|\varepsilon_i\|\,|\Delta v_i|+0.5\Delta v_i^2}{\|\zeta_{2i}\|^2}\zeta_{2i}+\Delta v_i & \\ \qquad\qquad \text{if } \|\zeta_{2i}\| \ge \chi_2 \quad (36)\\ 0 \qquad\qquad \text{if } \|\zeta_{2i}\| < \chi_2 \quad (37)\end{cases}$$

where $k_6 > 0$, χ_2 is a small positive value, and $\zeta_{2i} \in \mathbb{R}$ is the state of the auxiliary design system.

Theorem 1: Considering N mobile agents with similar dynamics (1), Assumptions 1–4 and formation control laws (21)–(26) and (33)–(37), and the selection of parameters satisfying that $k_1 > \max\{|\mathcal{E}_i|, 2(v_{\max}(1-|\mathcal{E}_i|)+\|\delta_{ij}\|\omega_{\max})/(|\mathcal{E}_i|\|\varepsilon_i\|)\}$, $k_2 > 0.5$, $k_4, k_6 > 1$, the predefined formation expressed in (8) will be achieved with bounded formation errors.

Proof of Theorem 1: See Appendix.

IV. Vision-Based Pose Estimation

In this section, a method to estimate the pose of an object using RGBD images captured by kinect will be proposed. The Microsoft Kinect combines 3-D depth map information with traditional RGB color camera data. The advantages of this sensor over stereo cameras are its low computational expense in calculating depth and the accuracy of the range measurements. The CamShift algorithm is applied to track a selected object, which can be implemented in real time, confirming the real-time performance of the control strategy.

To further obtain the required information to estimate the pose of the leader, the region of the kinect board in the leader is chosen as the region of interest (ROI) in the visual tracking algorithm. Fig. 2(a) demonstrates the visual-tracking outcome in Gazebo where the green line encloses the ROI and the red circle marks the centroid of the ROI. Then, the following information can be directed acquired from an RGBD image executing the object tracking algorithm: $\mathbf{r}_L = [x_L, y_L, d_L]$, $\mathbf{r}_M = [x_M, y_M, d_M]$, and $\mathbf{r}_R = [x_R, y_R, d_R]$ corresponding to the midpoint of the left border, the centroid, and the midpoint of the right border of the region tracked on the depth image, with the location $[x_L, y_L]$, $[x_M, y_M]$, and $[x_R, y_R]$, and the depth value d_L, d_M, and d_R.

Define L^r as the real length of the kinect on the local leader in the axis that the long side of the kinect of the follower lies on, while L^f is the length of the kinect of the local leader in the view of the follower. These variables have been marked in Fig. 2(b) and (c). Then, we have $L^f = x_R - x_L$ and $L^r = \kappa d_M L^f$, where $\kappa > 0$ is a scaling factor mapping lengths measured in pixel units to lengths measured in meters. The estimation of the orientation β_i with respect to the local leader frame $\mathcal{J}$ can be obtained as $\beta_i = \arctan((d_L - d_R)/L^r)$. Define $r_O = [x_O, y_O]$ as the centroid of the depth image and l^f as the horizontal offset in the depth image that $l^f = x_M - x_O$. Let l_i^r be the offset of the kinect center of the leader v_j to the kinect centroid of the follower v_i in the axis the long side of the kinect of the follower v_i lies on in real world, which can be estimated as $l_i^r = -\kappa d_M l^f = d_M \tan\gamma_i$ and we could infer that $\gamma_i = \arctan\left(-\kappa l^f\right)$, which further yields that

$$\alpha_i = \arctan\left(-\kappa l^f\right) + \arctan\left(\frac{d_L - d_R}{L^r}\right). \tag{38}$$

Then, the distance between the follower v_i and the local leader v_j can be obtained as $r_i = (d_M^2 + l_i^{r2})^{1/2}$. The follower v_i can be localized with respect to its local leader v_j as:

$$x_i = -r_i \cos\alpha_i \quad \& \quad y_i = -r_i \sin\alpha_i \tag{39}$$

inferring the formation error of the follower v_i as in the following:

$$\varepsilon_{xi} = -r_i \cos\alpha_i - \delta_{xi} \quad \& \quad \varepsilon_{yi} = -r_i \sin\alpha_i - \delta_{yi}. \tag{40}$$

With the help of variables acquired in this section, the control schemes proposed in Section III are able to be implemented without communication among agents or a laser range finder to determine the distance to the leader or a gyroscope to measure the orientation.

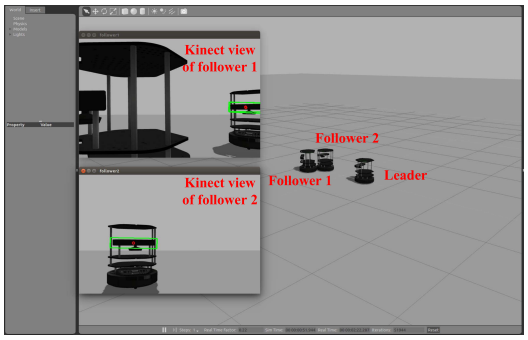

Fig. 3. Simulation interface.

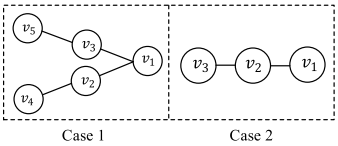

Fig. 4. Two formation topologies in Section V-A.

V. Simulation and Experiment Studies

The Turtlebot2 with Kinect for Xbox 360 is chosen as the agent in both simulation and experimental studies. The angular field of kinect view is 57° horizontally and 43° vertically. Only the horizontal view limit is considered in this brief; thus, we choose $\gamma_{\max} = 25°$ leaving a gap for safety and robustness issues. Moreover, kinect has a practical ranging limit of 3.5 m distance, and to further enable the visual tracking of the kinect to work during the whole task, a smaller value of distance limit should be adopted, which is set to be $r_{\max} = 2.0$ m. The settings of the parameters are: $k_1 = 0.6$, $k_2 = 0.8$, $k_4 = 1.1$, $k_6 = 1.1$, $\chi_1 = 0.001$, and $\chi_2 = 0.001$.

A. Simulations

A simulation platform for the formation control of MAS is developed using the Gazebo simulator on robot operating system (ROS) implemented by Python. To study the performance of control laws (21)–(24) and (33)–(35) as well as the pose estimation algorithm introduced in Section III, a simulation interface is designed as Fig. 3 with two subwindows illustrating the kinect view of two followers and a main window demonstrating the motion of three agents in the environment.

We will explore two formation topologies as shown in Fig. 4 that both contains two communication levels. The results are shown in Figs. 5–9.

In the first case, we consider the first topology where $N = 5$. MAS will generate Pseudo V formation topology tracking a straight path ($v_1 = 0.3$ and $\omega_1 = 0$), where v_1 is the leader for v_2 and v_3, v_2 is the local leader for v_4, and v_3 is the local leader for v_5. The configuration vectors for five agents in world coordinate system are initialized as $\mathbf{q}_{01} = [0 \;\; 0 \;\; 0]^T$, $\mathbf{q}_{02} = [-2.0 \;\; -0.25 \;\; 0]^T$, $\mathbf{q}_{03} = [-1.9 \;\; 0.5 \;\; 0]^T$, $\mathbf{q}_{04} = [-3.2 \;\; -0.8 \;\; 0]^T$, and $\mathbf{q}_{05} = [-3.3 \;\; 0.7 \;\; 0]^T$ [see Fig. 7(a)]. The desired formation position vectors for v_2 and v_4 with respect to the local leader

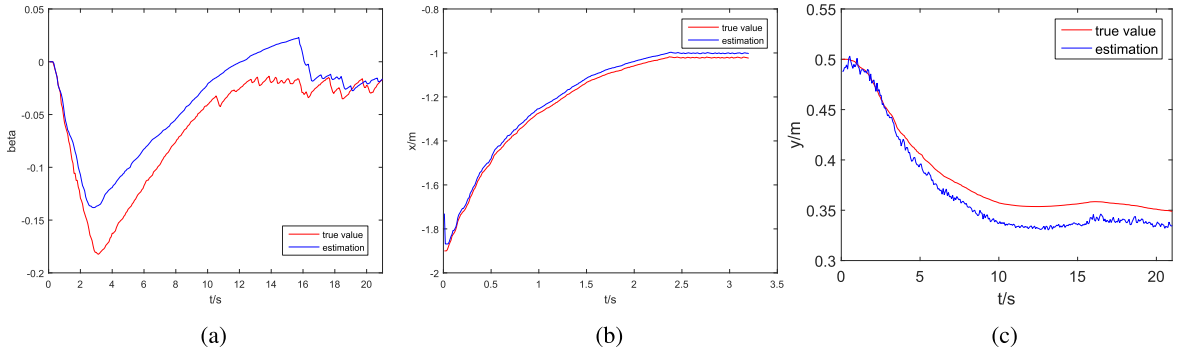

Fig. 5. Pose estimation results. (a) Relative orientation. (b) Relative position in x-coordinate. (c) Relative position in y-coordinate.

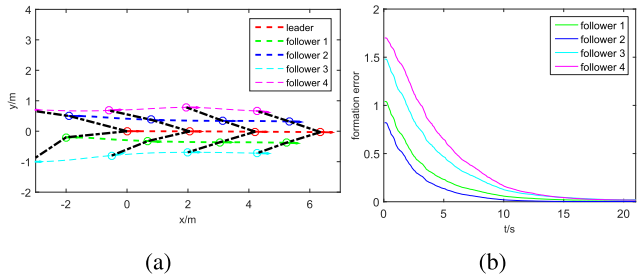

Fig. 6. Formation tracking results for the first case in Section V-A. (a) Trajectories for whole tacking process. (b) Time history of formation errors.

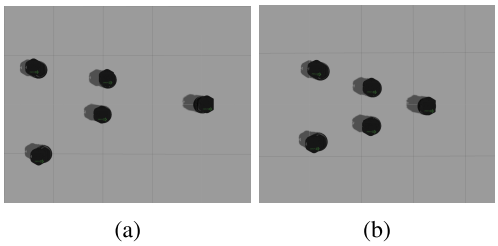

Fig. 7. Formation tracking results for the first case in Section V-A. (a) $t = 0$ s. (b) $t = 30$ s.

frame $\mathcal{J}$ are set as $\mathbf{r}_2^{\mathrm{d}} = [-1.0 \quad -0.4]^T$ and the ones for v_3 and v_5 are set as $\mathbf{r}_3^{\mathrm{d}} = [-1.0 \quad 0.4]^T$.

First, the effectiveness of vision-based algorithm for pose estimation is validated for the formation tracking with the first topology. The estimation for the relative orientation, relative positions in x-coordinate and y-coordinate of v_2 are illustrated in Fig. 5, while the true values are got from *Odometry* message source of the navigation stack in Turtlebot2 plotted in the figure for comparison. The sources of the estimation errors includes (i) kinect measurement error, and (ii) the estimation of the length scaled from pixels, etc.

Fig. 7(b) plots the positions of five agents at the end, where we could see the desired formation is realized. The whole tracking trajectories are illustrated in Fig. 6(a). The formation errors, which are calculated by *Odometry* message source of the navigation stack in Turtlebot2, decrease gradually to a small value with time as shown in Fig. 6(b). The main stabilization error sources for the formation tracking are: (i) the nonzero input for the leader agent; (ii) the estimation error.

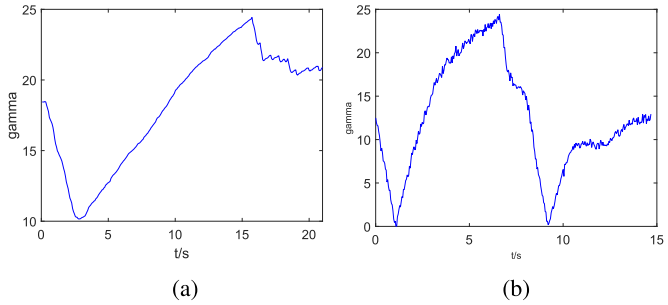

Fig. 8. Time history of $|\gamma_2|$. (a) Simulation. (b) Experiment.

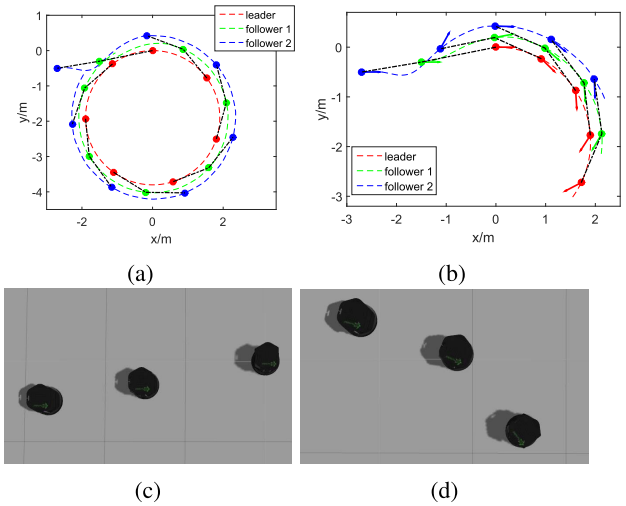

Fig. 9. Formation tracking results for the second case in Section V-A. (a) Trajectories for whole tacking process. (b) Trajectories for the beginning formation generation process. (c) $t = 0$ s. (d) $t = 8$ s.

The time history of $|\gamma_2|$ is demonstrated in Fig. 8(a), where it could be seen that $|\gamma_2|$ is controlled whin $\gamma_{\max} = 25°$. Two simulations also prove the effectiveness of visibility maintenance algorithms. The proposed visibility maintenance strategies guarantee the success of visual tracking and the connection of the sensing networks.

Similarly, in the second one, we consider the second topology where $N = 3$. A line formation topology will be achieved to track a circle path ($v_1 = 0.2$, $\omega_1 = 0.1$), where v_1 is the leader for v_2 and v_2 is the local leader for v_3. The configuration vectors for three agents in world coordinate system

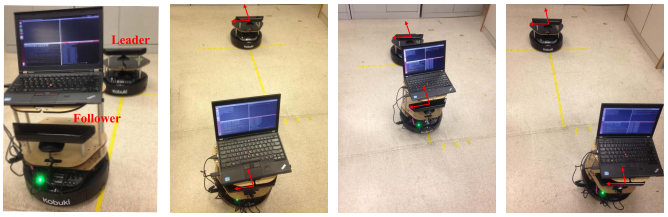

(a) (b) (c) (d)

Fig. 10. (a) Experimental setup. (b) Initialization. (c) Generation of first formation. (d) Generation of second formation.

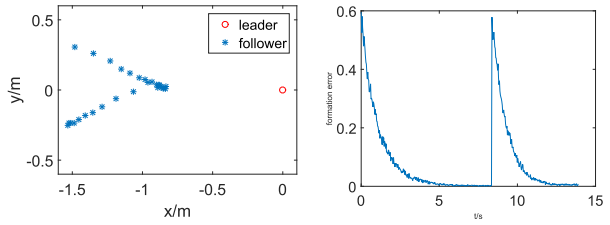

(a) (b)

Fig. 11. Experimental result. (a) Trajectory. (b) Formation error.

are initialized as $\mathbf{q}_{01} = [0 \quad 0 \quad 0]^T$, $\mathbf{q}_{02} = [-1.5 \quad -0.3 \quad 0]^T$, and $\mathbf{q}_{03} = [-2.7 \quad -0.5 \quad 0]^T$. The desired formation position vectors for v_2 and v_3 with respect to the leader frame $\mathcal{J}$ are set as $\mathbf{r}_2^{\mathrm{d}} = [-1.0 \quad 0]^T$ and $\mathbf{r}_3^{\mathrm{d}} = [-1.0 \quad 0]^T$.

The whole tracking trajectories are illustrated in Fig. 9(a), while the beginning formation generation phase is detailed in Fig. 9(b). Fig. 9(c) plots the initialized positions and orientations of three agents. Although the initialized positions seem to form a straight line in the world coordinate system, the displacement in y-coordinate with respect to the leader frame does not equal to zero. Fig. 9(d) illustrates the scene that the desired formation has been nearly achieved. Due to the nonzero angular velocity of the global leader v_1, the desired displacement on relative positions has been almost reached, although there is a small offset in the motion direction of the follower with respect to the local leader frame, which leads to a formation of broken line in world coordinate system rather than a straight line as designed.

B. Experiments

In order to test the proposed vision-based formation control strategy in a realistic scenario, a simple experiment is carried out at the Robotics Research Laboratory, National University of Singapore, Singapore. The experimental setup consists of two Turtlebots acting as the leader and the follower as shown in Fig. 10(a). The follower Turtlebot consists of a laptop (Thinkpad X230, Lenovo Inc.) with ROS, while there is no laptop connected to the leader Turtlebot proving no communication between two agents. The leader is chosen to be static in this experiment to observe the process of formation generation and formation error with zero input of the leader.

The configuration vectors for two agents in world coordinate system are initialized as $\mathbf{q}_{01} = [0 \quad 0 \quad 0]^T$ and $\mathbf{q}_{02} = [-1.5 \quad 0.3 \quad 0]^T$ [see Fig. 10(b)]. The desired formation position vector for v_2 with respect to the leader frame is set as $\mathbf{r}_2^{\mathrm{d}} = [-0.8 \quad 0]^T$. A switching signal will be manually sent after the first given formation has been formed, and then the desired formation position vector for $v_2$with respect to the leader frame is set as $\mathbf{r}_2^{\mathrm{d}} = [-1.5 \quad -0.3]^T$. Fig. 10(c) and (d) plots the scenes where the switching formations have been basically achieved. The trajectory of followers relative to the position of the leader and the time history of the formation error is illustrated in Fig. 11. The formation error decreases and remains close to zero approximately in $t \in [0, 8.4]s$. At around $t = 8.4$ s, there is an impulsive increase of the formation error due to the switching signal, then the given formation is achieved again at around $t = 14$ s. As expected, the zero input for the leader agent results in that the formation error is able to converge to zero. The time history of $|\gamma_2|$ is demonstrated in Fig. 8(b), where it could be seen that $|\gamma_2|$ is controlled with $\gamma_{\max} = 25°$ validating the effectiveness of visibility maintenance strategies in real environment. The slight vibration might come from the measurement error of the kinect, which caused by the shaking of the Turtlebot in the experiment.

VI. Conclusion

This brief has presented a kinect-based formation tracking control for MAS under visibility constraints. A pose estimation algorithm using RGBD images has been proposed to estimate the relative orientation and relative positions of the local leader. The proposal of the visual localization benefits the success of L-F formation without the communication among agents. The desired formation based on the given position displacement has been generated with the consensus in motion direction by the designed dipolar vector field. The visibility constraints, resulting from the limited vision range of the kinect used as the sole sensor for formation, have been converted into input constrains. Under the effect of the designed auxiliary system, the control protocol has been proved to achieve the formation tasks while maintaining the visibility constraints. Finally, simulation results using the Gazebo simulator on ROS as well as experimental results on Turtlebot2 have been presented to demonstrate the effectiveness of proposed approaches.

Compared with the achievements reported in [8], this brief has focused on the development of solution for the rigid formation for unicycle agent with the dynamics as shown in (1), since most of mobile robots are differentially driven. We aim for the displacement-based rigid formation and the consensus in the motion direction, which means that the positions of MAS should form a given shape, and more parameters should be estimated than the distance to describe the pose of the local leader accurately and maintain the visibility by limiting the control inputs. Compared with [14], the proposed strategies in this brief requires only one kinect or any cameras that can provide RGBD images, which will greatly improve the practicability.

Appendix

Proof of Theorem 1: Consider the Lyapunov candidate as $V_i = (1/2)\varepsilon_{xi}^2 + (1/2)\varepsilon_{yi}^2 + (1/2)(\beta_i - \varphi_i)^2 + (1/2)\zeta_{1i}^2 +$

$(1/2)\zeta_{2i}^2$, for $i = 2, \ldots, N$. The derivative of V_i is

$$\dot{V}_i = \varepsilon_{xi}\dot{\varepsilon}_{xi} + \varepsilon_{yi}\dot{\varepsilon}_{yi} + (\beta_i - \varphi_i)(\dot{\beta}_i - \dot{\varphi}_i) + \zeta_{1i}\dot{\zeta}_{1i} + \zeta_{2i}\dot{\zeta}_{2i}$$

with

$$\dot{\varepsilon}_{xi} = S(v_i)\cos\beta_i - v_j + y_i\omega_j \quad \& \quad \dot{\varepsilon}_{yi} = S(v_i)\sin\beta_i - x_i\omega_j.$$

We obtain that

$$\begin{aligned}\dot{V}_i &= [\varepsilon_{xi} \;\; \varepsilon_{yi}]\begin{bmatrix}\cos\beta_i \\ \sin\beta_i\end{bmatrix} S(v_i) + \zeta_{1i}\dot{\zeta}_{1i} \\ &\quad + (\beta_i - \varphi_i)(S(\omega_i) - \dot{\varphi}_i) + \zeta_{2i}\dot{\zeta}_{2i} \\ &\quad + [\varepsilon_{xi} \;\; \varepsilon_{yi} \;\; \beta_i - \varphi_i]\begin{bmatrix}-v_j + y_i\omega_j \\ -x_i\omega_j \\ -\omega_j\end{bmatrix}. \end{aligned} \tag{41}$$

Specifically, we define

$$P_1 \triangleq (\varepsilon_{xi}\cos\beta_i + \varepsilon_{yi}\sin\beta_i)S(v_i) + \zeta_{2i}\dot{\zeta}_{2i} \tag{42}$$

$$P_2 \triangleq (\beta_i - \varphi_i)(S(\omega_i) - \dot{\varphi}_i) + \zeta_{1i}\dot{\zeta}_{1i} \tag{43}$$

$$P_3 \triangleq [\varepsilon_{xi} \;\; \varepsilon_{yi} \;\; \beta_i - \varphi_i][-v_j + y_i\omega_j \;\; -x_i\omega_j \;\; -\omega_j]^T. \tag{44}$$

Denote $\mathcal{E}_i = (\varepsilon_i^T/\|\varepsilon_i\|)\left[\begin{smallmatrix}\cos\beta_i \\ \sin\beta_i\end{smallmatrix}\right]$ in the following. Substituting (35)–(37) into (42) yields that

$$\begin{aligned}P_1 &= -k_6\zeta_{2i}^2 - 0.5\Delta v_i^2 + \zeta_{2i}\Delta v_i - \|\varepsilon_i\|\,|\Delta v_i| \\ &\quad + (\varepsilon_{xi}\cos\beta_i + \varepsilon_{yi}\sin\beta_i)(v_i + \Delta v_i) \\ &\le -\left(k_1|\mathcal{E}_i| - 0.5\mathcal{E}_i^2\right)\|\varepsilon_i\|^2 - (k_6 - 1)\zeta_{2i}^2 \\ &\quad -\text{sgn}(\varepsilon_{xi})\,v_{\max}\left(\varepsilon_i^T\begin{bmatrix}\cos\beta_i \\ \sin\beta_i\end{bmatrix}\right). \end{aligned} \tag{45}$$

Substituting (24)–(26) into (43) yields that

$$\begin{aligned}P_2 &= -k_2(\beta_i - \varphi_i)^2 + (\beta_i - \varphi_i)(-\zeta_{1i} + \Delta\omega_i) - k_4\zeta_{1i}^2 \\ &\quad -0.5\Delta\omega_i^2 - |(\beta_i - \varphi_i)\Delta\omega_i| + \zeta_{1i}\Delta\omega_i \\ &\le -(k_2 - 0.5)(\beta_i - \varphi_i)^2 - (k_4 - 1)\zeta_{1i}^2 \end{aligned} \tag{46}$$

$$\begin{aligned}P_3 &\le \|\varepsilon_i\|\,v_{\max} + [\varepsilon_{xi} \;\; \varepsilon_{yi}]\begin{bmatrix}\varepsilon_{yi} + \delta_{yi} \\ -\varepsilon_{xi} - \delta_{xi}\end{bmatrix}\omega_j - (\beta_i - \varphi_i)\omega_j \\ &= \|\varepsilon_i\|\,v_{\max} + \varepsilon_i^T\begin{bmatrix}\delta_{yi} \\ -\delta_{xi}\end{bmatrix}\omega_j - (\beta_i - \varphi_i)\omega_j \\ &\le \|\varepsilon_i\|(v_{\max} + \|\delta_i\|\omega_{\max}) + |(\beta_i - \varphi_i)|\,\omega_{\max}. \end{aligned} \tag{47}$$

Let $\vartheta_i = \beta_i - \varphi_i$, representing the dynamics of the orientation error of v_i, we have $\dot{\vartheta}_i = \dot{\beta}_i - \dot{\varphi}_i = \dot{\theta}_i - \dot{\theta}_j - \dot{\varphi}_i = \omega_i - \omega_j - \dot{\varphi}_i = -k_2(\beta_i - \varphi_i) - \omega_j = -k_2\vartheta_i - \omega_j \le -k_2\vartheta_i + \omega_{\max}.$, yielding that $\vartheta \le \vartheta_i(0) + (\omega_{\max}/k_2)$. Therefore, P_3 can be further written as $P_3 \le \|\varepsilon_i\|(v_{\max} + \|\delta_i\|\omega_{\max}) + (\omega_{\max}^2/k_2) + \vartheta_i(0)\omega_{\max}$. Let $\xi_i = \vartheta_i(0)\omega_{\max} + (\omega_{\max}^2)(k_2)$, (41) can be rewritten as

$$\begin{aligned}\dot{V}_i &\le -0.5\left(k_1|\mathcal{E}_i| - \mathcal{E}_i^2\right)\|\varepsilon_i\|^2 - (k_2 - 0.5)(\beta_i - \varphi_i)^2 \\ &\quad + \|\varepsilon_i\|[v_{\max}(1 - |\mathcal{E}_i|) + \|\delta_{ij}\|\omega_{\max} - 0.5k_1|\mathcal{E}_i|\,\|\varepsilon_i\|] \\ &\quad - (k_4 - 1)\zeta_{1i}^2 - (k_6 - 1)\zeta_{2i}^2 + \xi_i. \end{aligned} \tag{48}$$

By properly choosing parameters, e.g., satisfying that $k_1 > \max\{|\mathcal{E}_i|, 2(v_{\max}(1 - |\mathcal{E}_i|) + \|\delta_{ij}\|\omega_{\max})/(|\mathcal{E}_i|\,\|\varepsilon_i\|)\}$, $k_2 > 0.5$, $k_4, k_6 > 1$, we can obtain that $\dot{V}_i \le -k_v V_i + \xi_i$, where $k_v = \min\{k_1|\mathcal{E}_i| - \mathcal{E}_i^2, 2k_2 - 1, 2k_4 - 2, 2k_6 - 2\}$. Let $\varrho_i \triangleq \xi_i/k_v$, it follows that $0 \le V_i(t) \le [V_i(0) - \varrho_i]e^{-k_v t} \le V_i(0) + \varrho_i$, which further derives that $\|\varepsilon_i(t)\| \le (2V_i(t))^{1/2} \le (2V_i(0) + 2\varrho_i)^{1/2}$. Hence, MAS will be asymptotic stable, and the desired L-F formation tracking will be achieved with bounded formation errors under visibility constraints. ■

REFERENCES

[1] Y. Lyu, Q. Pan, C. Zhao, Y. Zhang, and J. Hu, "Vision-based UAV collision avoidance with 2D dynamic safety envelope," *IEEE Aerosp. Electron. Syst. Mag.*, vol. 31, no. 7, pp. 16–26, Jul. 2016.

[2] R.-J. Wai and Y.-W. Lin, "Adaptive moving-target tracking control of a vision-based mobile robot via a dynamic Petri recurrent fuzzy neural network," *IEEE Trans. Fuzzy Syst.*, vol. 21, no. 4, pp. 688–701, Aug. 2012.

[3] A. K. Das, R. Fierro, V. Kumar, J. P. Ostrowski, J. Spletzer, and C. J. Taylor, "A vision-based formation control framework," *IEEE Trans. Robot. Autom.*, vol. 18, no. 5, pp. 813–825, Oct. 2002.

[4] D. Panagou and V. Kumar, "Cooperative visibility maintenance for leader–follower formations in obstacle environments," *IEEE Trans. Robot.*, vol. 30, no. 4, pp. 831–844, Aug. 2014.

[5] X. Chen and Y. Jia, "Adaptive leader-follower formation control of non-holonomic mobile robots using active vision," *IET Control Theory Appl.*, vol. 9, no. 8, pp. 1302–1311, 2015.

[6] G. L. Mariottini *et al.*, "Vision-based localization for leader–follower formation control," *IEEE Trans. Robot.*, vol. 25, no. 6, pp. 1431–1438, Dec. 2009.

[7] E. Montijano, E. Cristofalo, D. Zhou, M. Schwager, and C. Sagüés, "Vision-based distributed formation control without an external positioning system," *IEEE Trans. Robot.*, vol. 32, no. 2, pp. 339–351, Apr. 2016.

[8] B. Fidan, V. Gazi, S. Zhai, N. Cen, and E. Karataş, "Single-view distance-estimation-based formation control of robotic swarms," *IEEE Trans. Ind. Electron.*, vol. 60, no. 12, pp. 5781–5791, Dec. 2013.

[9] P. Vela, A. Betser, J. Malcolm, and A. Tannenbaum, "Vision-based range regulation of a leader-follower formation," *IEEE Trans. Control Syst. Technol.*, vol. 17, no. 2, pp. 442–448, Mar. 2009.

[10] A. Lopez-Gonzalez, E. D. Ferreira, E. G. Hernandez-Martinez, J.-J. Flores-Godoy, G. Fernandez-Anaya, and P. Paniagua-Contro, "Multi-robot formation control using distance and orientation," *Adv. Robot.*, vol. 30, no. 14, pp. 901–913, 2016.

[11] E. D. Ferreira-Vazquez, E. G. Hernandez-Martinez, J.-J. Flores-Godoy, G. Fernandez-Anaya, and P. Paniagua-Contro, "Distance-based formation control using angular information between robots," *J. Intell. Robot. Syst.*, vol. 83, nos. 3–4, pp. 543–560, 2016.

[12] C. T. Recchiuto, A. Sgorbissa, and R. Zaccaria, "Visual feedback with multiple cameras in a UAVs human–swarm interface," *Robot. Auto. Syst.*, vol. 80, pp. 43–54, Jun. 2016.

[13] R. Li and Y. Li, "Localization of leader-follower formations using Kinect and RTK-GPS," in *Proc. IEEE Int. Conf. Robot. Biomimetics (ROBIO)*, Dec. 2014, pp. 908–913.

[14] X. Liang, Y.-H. Liu, H. Wang, W. Chen, K. Xing, and T. Liu, "Leader-following formation tracking control of mobile robots without direct position measurements," *IEEE Trans. Autom. Control*, vol. 61, no. 12, pp. 4131–4137, Dec. 2016.

[15] X. Chen and Y. Jia, "Input-constrained formation control of differential-drive mobile robots: Geometric analysis and optimisation," *IET Control Theory Appl.*, vol. 8, no. 7, pp. 522–533, 2014.

[16] W. Chung *et al.*, "Safe navigation of a mobile robot considering visibility of environment," *IEEE Trans. Ind. Electron.*, vol. 56, no. 10, pp. 3941–3950, Oct. 2009.

[17] G. Allibert, E. Courtial, and F. Chaumette, "Predictive control for constrained image-based visual servoing," *IEEE Trans. Robot.*, vol. 26, no. 5, pp. 933–939, Oct. 2010.

[18] S. M. LaValle, *Planning Algorithms*. Cambridge, U.K.: Cambridge Univ. Press, 2006.

[19] M. Chen, S. S. Ge, and B. Ren, "Adaptive tracking control of uncertain MIMO nonlinear systems with input constraints," *Automatica*, vol. 47, no. 3, pp. 452–465, Mar. 2011.